Immunoassay platform with surface-enhanced resonance Raman scattering for detecting trace levels of SARS-CoV-2 spike protein

Maria J. Bistaffa [a],[1], Sabrina A. Camacho [a],[b],[*],[1], Wallance M. Pazin [b],[c], Carlos J.L. Constantino [c], Osvaldo N. Oliveira Jr. [b], Pedro H.B. Aoki [a]

[a] São Paulo State University (UNESP), School of Sciences, Humanities and Languages, Assis, SP, 19806-900, Brazil
[b] IFSC, São Carlos Institute of Physics, University of São Paulo (USP), São Carlos, SP, 13566-590, Brazil
[c] São Paulo State University (UNESP), School of Technology and Applied Sciences, 19060-900, Presidente Prudente, SP, Brazil

ARTICLE INFO

ABSTRACT

The early diagnosis of Coronavirus disease (COVID-19) requires either an accurate detection of genetic material or a sensitive detection of viral proteins. In this work, we designed an immunoassay platform for detecting trace levels of SARS-CoV-2 spike (S) protein. It is based on surface-enhanced resonance Raman scattering (SERRS) of methylene blue (MB) adsorbed onto spherical gold nanoparticles (AuNPs) and coated with a 6 nm silica shell. The latter shell in the SERRS nanoprobe prevented aggregation and permitted functionalization with SARS-CoV-2 antibodies. Specificity of the immunoassay was achieved by combining this functionalization with antibody immobilization on the cover slides that served as the platform support. Different concentrations of SARS-CoV-2 antigen could be distinguished and the lack of influence of interferents was confirmed by treating SERRS data with the multidimensional projection technique Sammon's mapping. With SERRS using a laser line at 633 nm, the lowest concentration of spike protein detected was 10 pg/mL, achieving a limit of detection (LOD) of 0.046 ng/mL (0.60 pM). This value is comparable to the lowest concentrations in the plasma of COVID-19 patients at the onset of symptoms, thus indicating that the SERRS immunoassay platform may be employed for early diagnosis.

1. Introduction

Early diagnosis of the Severe Acute Respiratory Syndrome Coronavirus 2 (SARS-CoV-2) [1–3] is efficient to prevent the fast spreading of the virus by inhibiting human-human transmission through direct routes [4–6]. The most used detection method has been reverse transcription-polymerase chain reaction (RT-PCR). The test consists in converting the viral mRNA into DNA and applying PCR reactions to DNA amplification and detection [7,8]. RT-PCR is highly specific for SARS-CoV-2, but its accuracy may be compromised by variations in sample collection and persistence of viral RNA in the nasal cavity/throat, thus leading to false-negative/false-positive results [9–12]. Additionally, PCR involves multiple sample processing steps (e.g., nucleic acid extraction, purification, and amplification), making it time-consuming and expensive [13]. The other types of widely used tests are serological tests [14–16], which are more stable than viral RNA tests owing to the uniform distribution of proteins in the blood, tending to

reduce false-negatives [17]. However, these tests to detect SARS-CoV-2 antibodies via enzyme-linked immunosorbent assays (ELISA) [12, 18–20] or lateral flow immunoassays (LFAs) [21] cannot be used for early diagnosis. Indeed, it can take 2–3 weeks for viral-specific antibodies to be produced after infection.

Biosensors with distinct architectures have been developed for early detection of Coronavirus disease (COVID-19), with the spike protein being the most used biomolecule for diagnosis. For instance, Soares et al. [22] developed an immunosensor made of carboxymethyl chitosan coated with an active layer of specific antibodies, capable to detect the spike protein via electrical impedance spectroscopy. The spike protein could also be detected in sensing chips containing metamaterials and using terahertz time-domain spectroscopy [23], and with magnetic microrobots immuno-sandwich assays [24]. For diagnosis of COVID-19 through detection of nucleocapsid protein, Chen et al. [25] constructed an electrical double layer biosensor, while Qi et al. [26] designed a fast-responding aptasensor based on a low-cost microelectrode array
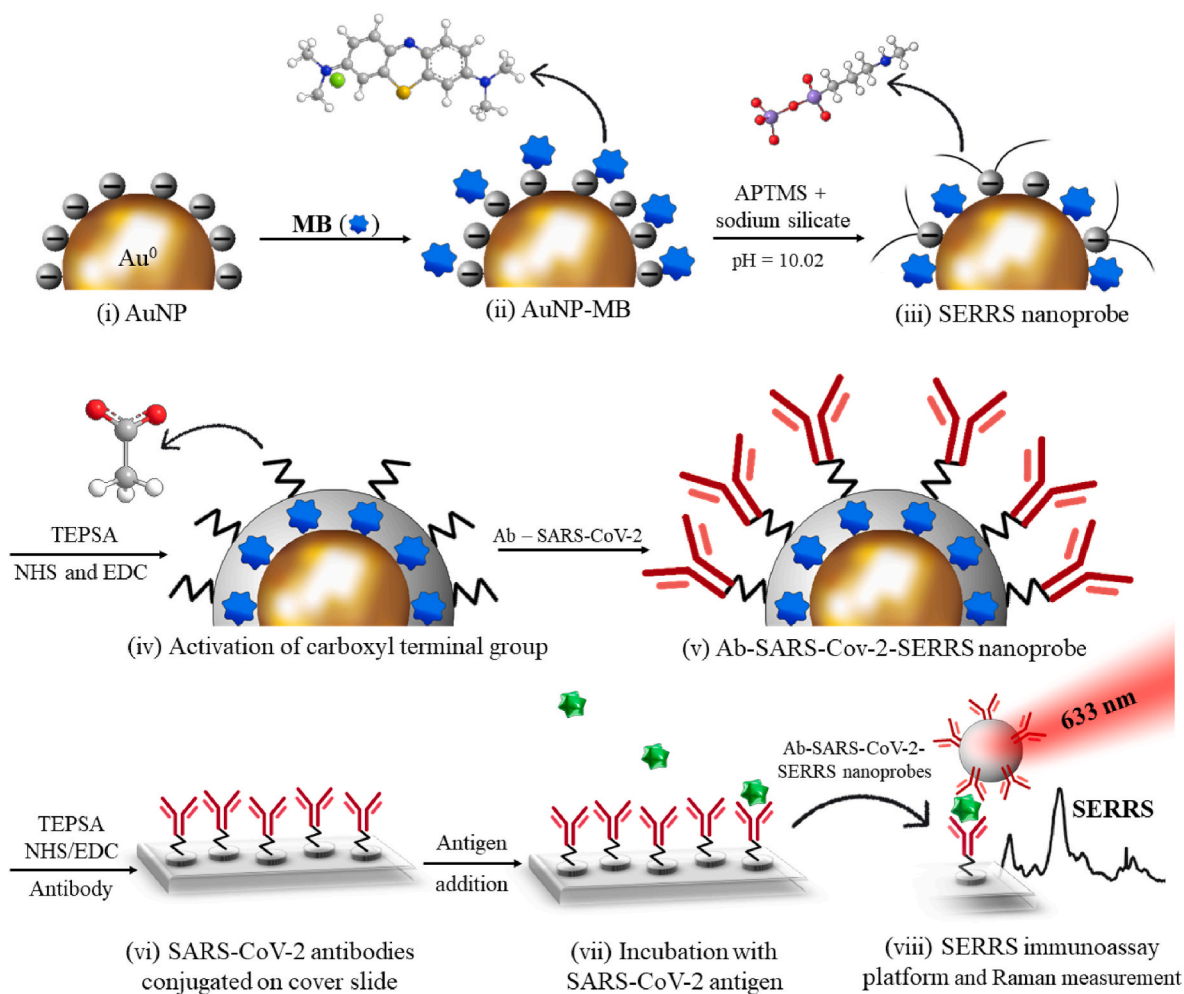
Scheme 1. Illustration of the design of Ab-SARS-CoV-2-SERRS nanoprobes: (i) AuNP (ca. 14 nm diameter) prepared via citrate reduction; (ii) AuNP bonded with MB molecules, whose 3D molecular structure is indicated by the arrow; (iii) AuNP + MB molecules + an ultrathin silica shell (SERRS nanoprobe – ca. 6 nm shell thickness) where the amino group of APTMS is firstly bonded to the negative charge surrounding the AuNP followed by sodium silicate binding with APTMS, forming the 3D complex molecular structure indicated by the arrow; (iv) activation of carboxyl terminal groups; (v) functionalization with Ab-SARS-CoV-2 (Ab-SARS-CoV-2-SERRS nanoprobe (ca. 31 nm); (vi) functionalization of the cover slide with SARS-CoV-2 antibodies; (vii) incubation of SARS-CoV-2 antigen onto the cover slide already functionalized with SARS-CoV-2 antibodies in the previous step; and (viii) incubation with Ab-SARS-CoV-2-SERRS nanoprobes completing the SERRS immunoassay platform, followed by Raman measurement.

chip. RNA fragments have also been applied in detecting Covid-19 with a one-pot loop probe-mediated isothermal amplification method [27]. There are serological tests which can be used for early diagnosis, for they can detect viral proteins at the onset of symptoms. For instance, SARS-CoV-2 spike (S1) protein was detected in the plasma of COVID-19 patients at concentrations ranging from ~8 to 20,000 pg/mL [28], thus permitting an accurate and early detection of COVID-19. One important requirement to achieve high accuracy is the capability to detect trace levels of such proteins. This motivates the search for highly sensitive methods, such as surface-enhanced resonance Raman scattering (SERRS) to detect the target molecule adsorbed on plasmonic metallic nanostructures [29,30]. SERRS has been used to detect trace level concentrations of neurotransmitters [31], proteins [32–34], pesticides [35–37], heavy metal ions [38], and cancer biomarkers [33,34,39]. Combining SERRS with an immunoassay platform may allow one to detect different proteins and increase sensitivity [40,41].

In this paper, we report on an immunoassay platform for early diagnosis of Covid-19 with SARS-CoV-2 spike glycoprotein (S1) (antigen) used as target molecule. Gold nanoparticles (AuNPs) were conjugated with methylene blue (MB) enclosed by a silica layer to avoid uncontrolled aggregation and chemical degradation. MB is a Raman reporter molecule, whose absorption is in resonance with the excitation

laser line (at 633 nm), with which one may generate surface-enhanced resonance Raman scattering (SERRS). The specificity to the immunoassay platform was warranted by functionalizing the nanoparticle (SERRS nanoprobe) with SARS-CoV-2 antibodies. These Ab-SARS-CoV-2-SERRS nanoprobes can detect concentrations of SARS-CoV-2 spike protein down to 10 pg/mL.

2. Materials and methods

2.1. Surface-enhanced Resonance Raman scattering (SERRS) nanoprobes

Spherical gold nanoparticles (AuNPs) with ca. 14 ± 3 nm diameter were synthesized via citrate reduction [42]. The procedure consisted in preparing 150×10^{-3} L tetrachloroauric acid (HAuCl$_4$ 0.5×10^{-3} mol/L; ref: 520918, Sigma-Aldrich, Saint-Louis, MO, USA) under vigorous stirring and boiling 7.5×10^{-3} L sodium citrate (38.8×10^{-3} mol/L; ref: S4641, Sigma-Aldrich). After the color change from yellow to reddish-purple, the colloidal suspension was maintained under heating for 10 min, and for an additional 15 min only under magnetic stirring. 0.5×10^{-3} L methylene blue (MB) (1.77×10^{-5} mol/L; ref: M9140, Sigma-Aldrich) were then mixed with 50×10^{-3} L AuNPs (1.1×10^{12} AuNPs/mL, concentration estimated as shown in the Supplementary
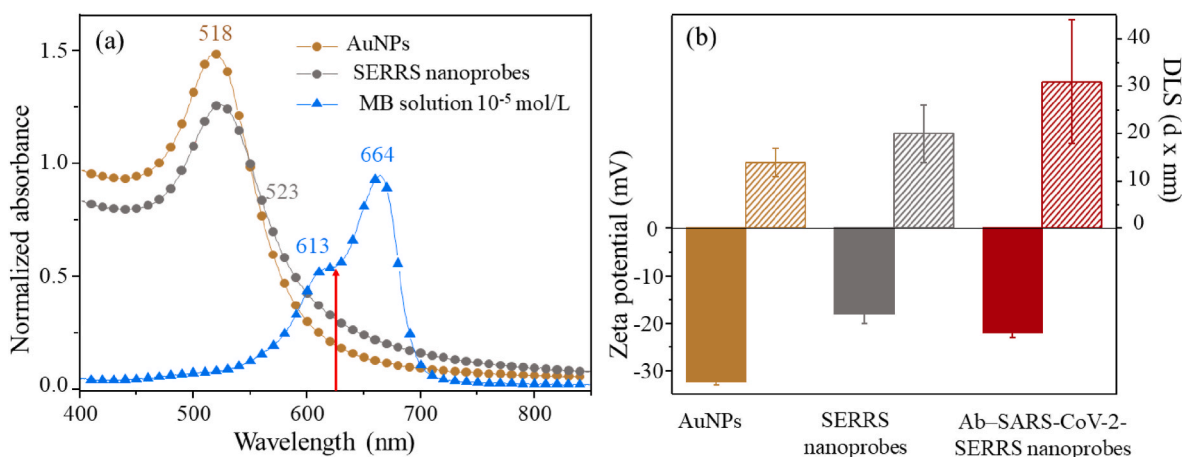
Fig. 1. (a) UV–Vis absorption spectrum of MB solution at 10^{-5} mol/L (blue) and UV–Vis extinction spectra of AuNPs (gold yellow) and SERRS nanoprobes (gray). The red arrow at 633 nm illustrates the excitation laser line applied in the resonance Raman experiments. (b) Zeta potential values and hydrodynamic diameters obtained with dynamic light scattering (DLS) for AuNPs, SERRS nanoprobes and Ab-SARS-CoV-2-SERRS nanoprobes. (For interpretation of the references to color in this figure legend, the reader is referred to the Web version of this article.)

Material) for 30 min under vigorous stirring at room temperature. The addition of MB allows for chemical adsorption [43,44] to establish a covalent bond through the N–CH$_3$ group from MB with the AuNP surface. AuNPs were subsequently coated with an ultrathin silica shell (about ca. 6 nm) by adding 3×10^{-3} L (3-aminopropyl) trimethoxysilane (APTMS 1×10^{-3} mol/L; ref 281778, Sigma-Aldrich) and stirred for 10 min before adding 6×10^{-3} L sodium silicate solution (0.54%, pH= 10; ref 338443, Sigma- Aldrich). The temperature of the system was raised to 90–95 °C and maintained for 3 h [45,46]. The silica coating prevents aggregation while providing an outstanding surface for further functionalization [47,48]. The final nanomaterial, made of AuNPs conjugated with MB molecules followed by a silica shell (AuNPs-MB@SiO$_2$), was named SERRS nanoprobe. 12×10^{-3} L SERRS nanoprobes were centrifuged at 14676 *g* for 15 min and redispersed into 1×10^{-3} L Milli-Q water (resistivity 18.2 MΩ.cm^{-1}) to obtain concentrated SERRS nanoprobes (1.1×10^{13} AuNPs-MB@SiO$_2$/mL). The colloidal suspensions were characterized using UV–Vis absorption spectroscopy (Agilent spectrometer, Cary 60, from 190 to 1100 nm), dynamic light scattering (DLS) and zeta potential measurements (Malvern Panalytical, model Zetasizer Nano S90). A schematic illustration of the preparation of SERRS nanoprobes is shown in Scheme 1.

2.2. Functionalization of SERRS nanoprobes with SARS-CoV-2 antibodies

The SERRS nanoprobes were functionalized with SARS-CoV-2 antibodies by adapting established protocols [47,48]. 1×10^{-3} L SERRS nanoprobes (1.1×10^{13} SERRS nanoprobes/mL) were diluted in 2.5×10^{-3} L Milli-Q water and incubated overnight with 2.5×10^{-3} L (3-triethoxysilyl) propylsuccinic anhydride (TEPSA 0.12 mol/L; ref: 094958, StartBioScience, Valinhos, SP, Brazil). The SERRS nanoprobes were rinsed with PBS solution and resuspended in 5×10^{-3} L N-hydroxysuccinimide (NHS 7.5×10^{-4} mol/L; ref 130672, Sigma-Aldrich) and N-(3-(dimethylamino)propyl)-N′-ethylcarbodiimide hydrochloride (EDC 3×10^{-3} mol/L; ref 03450, Sigma-Aldrich) PBS solution (ref: 4417, Sigma-Aldrich), in order to activate the carboxyl terminal groups from TEPSA. After 2 h, the SERRS nanoprobes were rinsed with PBS solution, redispersed in 5×10^{-3} L SARS-CoV-2 spike glycoprotein (S1) antibody (1.5×10^{-6} g/mL in PBS; ref: ab273073, ABCam, Cambrige, CA, USA) and incubated overnight in a refrigerator (4 °C) under magnetic stirring. A discussion on the estimated number of antibodies covering SERRS nanoprobe is included in the Supplementary Material. Lastly, the Ab-SARS-CoV-2-SERRS nanoprobes were centrifuged at 1500 *g* for 10 min and redispersed into 500×10^{-6} L PBS solution, removing unbounded antibodies. The colloidal suspension was

kept in a refrigerator (4 °C) for further SERRS immunoassay experiments. The functionalization of SERRS nanoprobes with SARS-CoV-2 antibodies is also illustrated in Scheme 1.

2.3. Functionalization of SARS-CoV-2 antibodies on cover slides

SARS-CoV-2 spike glycoprotein (S1) antibodies were functionalized on the surface of cover slides following published protocols [43,47,48]. This antibody immobilization onto the cover slides is essential to ensure the effectiveness of the immunoassay platform. For the specific antibody-antigen interaction prevents the antigens to be added in the next step from being removed in the rinsing step with PBS solution. The cover slides were cleaned with Milli-Q water and ethanol in an ultrasonic bath for 10 min each and incubated overnight with an ethanolic solution of TEPSA (0.1 mol/L). A parafilm® surface containing punched wells (0.6 mm of diameter) was placed onto each cover slide to predefine the immunoassay spots. Each punched-well contained a solution with either no antigen ("blank") or a given SARS-CoV-2 antigen concentration. For activating the carboxyl terminal groups from TEPSA, each immunoassay spot received 20×10^{-6} L NHS (1.5×10^{-4} mol/L) and EDC (3×10^{-3} mol/L) PBS solutions for 2 h. The antigens are therefore amenable to bind the SARS-CoV-2 antibodies on the cover slides. Then, the spots were rinsed with PBS and incubated overnight (in a refrigerator at 4 °C) with 15×10^{-6} L SARS-CoV-2 antibodies (2.4×10^{-4} g/mL in PBS). The functionalization of SARS-CoV-2 antibodies on cover slides is also displayed in Scheme 1.

2.4. SERRS immunoassay platform

The concentrations of recombinant human coronavirus SARS-CoV-2 spike glycoprotein (S1) (SARS-CoV-2 antigen; ref: ab273068, ABCam) were chosen based on the clinical appeal for COVID-19 diagnosis [49, 50], from 100 μg/mL to 0.01 ng/mL. An aliquot with 15×10^{-6} L of each antigen concentration was placed on the immunoassay spot of the cover slide, incubated for 1 h and rinsed with PBS solution. 15×10^{-6} L Ab-SARS-CoV-2-SERRS nanoprobes were added, incubated for an additional 1 h, and rinsed with PBS. After drying, the SERRS immunoassay platform was placed in Petri dishes and stored in refrigerator (4 °C) before use for the Raman measurements. The addition steps of SARS-CoV-2 antigen and Ab-SARS-CoV-2-SERRS nanoprobes as well as the Raman measurement and SERRS spectra collection are represented in Scheme 1. The possible effect of interferents was also verified using pharmaceutical drugs commonly taken by patients at the onset of COVID-19 symptoms or even without suspicion of COVID-19. Some of
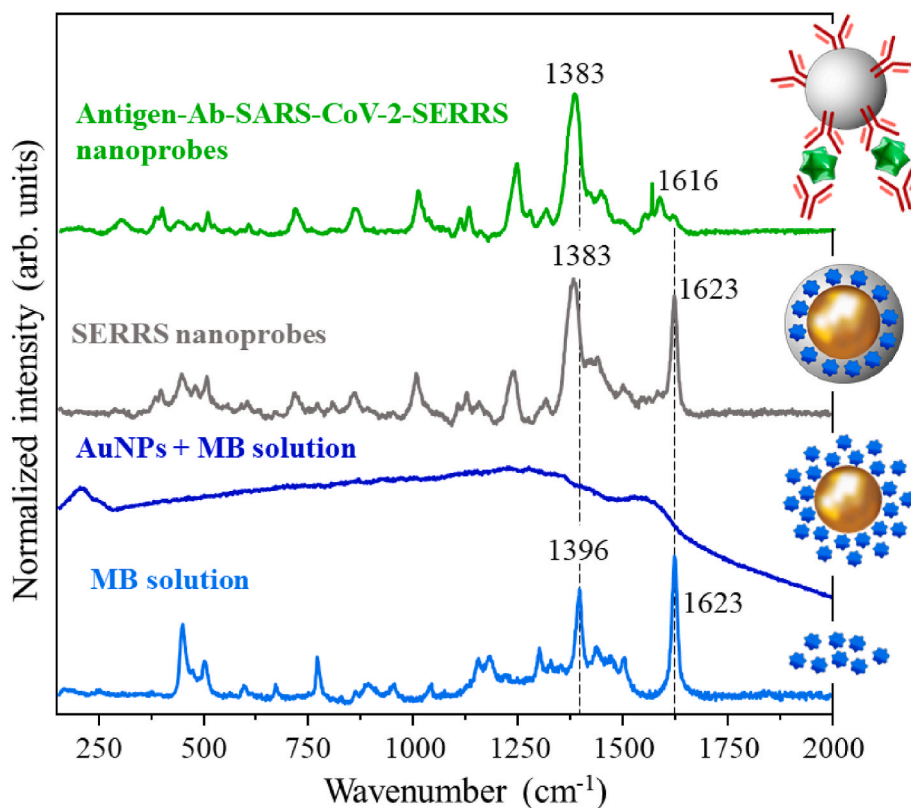
Fig. 2. Resonant Raman spectrum of 10^{-5} mol/L MB solution (blue); fluorescence spectrum of 10^{-5} mol/L MB solution containing AuNPs (dark blue); SERRS spectra of SERRS nanoprobes (gray) and antigen-Ab-SARS-CoV-2-SERRS nanoprobes (green) colloidal suspensions. The solutions and colloids were dropped on cover slides and let dry, thus forming drop-cast films which were analyzed via Raman spectroscopy. Excitation laser line at 633 nm. The fluorescence background was corrected in the SERRS spectra. (For interpretation of the references to color in this figure legend, the reader is referred to the Web version of this article.)

these drugs are now known as ineffective for COVID-19, though widely taken. The interferents used were paracetamol (750 mg; EMS, Brazil), azithromycin (500 mg; Eurofarma, Brazil), dexamethasone (4 mg; EMS, Brazil) and ivermectin (6 mg; Germed, Brazil). The aliquots of antigen were replaced by aliquots of the interferents and by aliquots of interferent + antigen. The interferents were tested separately and in a mixture, with and without antigen.

2.5. Resonance Raman, SERRS measurements and data analysis

The resonance Raman and SERRS spectra were acquired using an in-Via Raman microscope (Renishaw Inc., Hoffman Estates, IL) equipped with a 633 nm laser line, 1800 lines/mm diffraction grating, 10 s acquisition time, laser power attenuated to 10%, and a 50 × (NA = 0.75) dry objective (Leica Microsystems). SERRS mapping was carried out by selecting a 40 × 40 μm^2 area with 3 μm step, thus obtaining a total of 196 spectra for each mapped concentration. The baseline correction and analysis of Raman spectra was performed using Origin Pro V8.5 software (OriginLab Corporation, Northants). The data were also evaluated using the multidimensional projection technique referred to as Sammon's mapping [51,52]. With this methodology data from a multidimensional space are projected onto a 2D space trying to preserve similarity relationships within the original data set.

3. Results and discussion

As depicted in the schematic illustration of the Ab–SARS-CoV-2-SERRS nanoprobe in Scheme 1, methylene blue (MB) molecules are embedded between spherical gold nanoparticles (AuNPs) and ultrathin silica shells via covalent bond of N–CH₃ groups from MB with AuNPs, followed by functionalization with SARS-CoV-2 antibodies. The silica coating precludes aggregation and the leaching of MB during processing and assay operations. Furthermore, it provides an outstanding surface functionalization to render molecular specificity to the nanoprobes [43].

The UV–Vis absorption spectrum of the MB solution at 10^{-5} mol/L and the extinction spectra of AuNPs and SERRS nanoprobes are shown in Fig. 1(a). Two absorption peaks at 613 and 664 nm in the MB spectrum are assigned to n-π* transitions (n is the free doublet on the nitrogen atom of C=N bond and free doublet of S atom on S=C bond) [53]. The extinction of the localized surface plasmon resonance (LSPR) shifted from 518 nm (AuNPs) to 523 nm (SERRS nanoprobes) owing to the conjugated MB and silica shell covering the AuNP [43,47,48]. The zeta potential and hydrodynamic diameters for AuNPs, SERRS nanoprobes and Ab–SARS-CoV-2-SERRS nanoprobes are displayed in Fig. 1(b). AuNPs have approximately 14 ± 3 nm diameter, which increased to 20 ± 6 nm with the MB conjugation + silica coating and to 31 ± 13 nm with the functionalization of SARS-CoV-2 antibodies. The zeta potential was also affected, especially from the AuNPs (−32.4 ± 0.6 mV) to the SERRS nanoprobes (−18 ± 2 mV), whose increase is related to the reduction of negative charges around the nanoparticles. The AuNPs synthesized via citrate are negatively charged [42] and the cationic MB [54] and inert silica shell [55,56] decrease the surface charge. After functionalization with the antibodies a slight decrease is noted in zeta potential (−22 ± 1 mV). The prevalence of disulfide bonds and carboxyl-terminal groups in relation to amino-terminal groups in the antibody structure might lead to an increase of negative charges [57].

Fig. 2 shows the resonance Raman spectrum of MB solution at 10^{-5} mol/L, the fluorescence spectrum of MB solution (10^{-5} mol/L) containing AuNPs, the SERRS spectra of SERRS nanoprobes, and SERRS nanoprobes functionalized with Ab-SARS-CoV-2 and exposed to 1 μg/mL SARS-CoV-2 antigen. The latter corresponds to the complete immunoassay platform (cover slide functionalized with SARS-CoV-2 antibodies + antigen + Ab-SARS-CoV-2-SERRS nanoprobes, referred to as antigen-Ab-SARS-CoV-2-SERRS nanoprobes). Those experiments were carried out by dropping a given volume of the solutions or colloidal suspensions on glass cover slides, which were dried in a vacuum system. The assignments of the MB main vibrational modes from the Raman and SERRS spectra of Fig. 2 are displayed in Table 1. The MB solution (10^{-5}

Table 1

Assignments of the main vibrational modes from MB in solution (10^{-5} mol/L) and forming both SERRS nanoprobe and antigen-Ab-SARS-CoV-2-SERRS nanoprobe.

Ref	Wavenumber (cm^{-1})	MB (10^{-5} mol/L)	SERRS nanoprobe	Antigen-Ab-SERRS nanoprobe
[54, 67]	ν(C–C) ring	1623	1623	1616
				1583
		1502	1502	
[67]	ν_{asym} (C–N)		1438	1440
[54, 68]	ν_{sym} N–CH$_3$	1396	1382	1383
[69]	−CH2 twist		1316	1312
[68]	α(C–H)	1301		
				1273
				1241
			1237	
[67]	ν(C–N)	1180		
[70]	C–C (vibration)	1155	1158	
[67]	γ(C–H)		1127	1127
[54, 67]	β(C–H)	1038		
			1106	1106
[70]	C–C (rocking)		1006	1006
		950		
		944		
		891		
		860	860	860
			806	
[68]	β(C–H)	769		
			714	714
[67]	γ(C–H)	671		
			602	602
		596		
[67]	δ(C–N–C)	501	505	505
			478	478
		472		
[67, 71]	δ(C–N–C)	447	445	445
			395	395
			382	
				300

ν, stretching; α, in-plane ring deformation; β, in-plane bending; γ, out-of-plane bending; and δ, skeletal deformation.

mol/L) containing AuNPs (dark blue) yielded a fluorescence spectrum instead of SERRS signal. In fact, the MB molecules adsorbed on AuNPs might undergo fluorescence quenching [58] while forming a protective barrier that avoids the direct contact between the outermost MB molecules and the AuNPs surface. This protective barrier made of MB molecules provides a metal-dye distance that allows a continuous transition from fluorescence quenching to fluorescence enhancement [59,60]. On the other hand, in the SERRS nanoprobes spectrum (gray) the Raman fingerprint from MB is clear [54,61], with a slightly modified spectral profile compared with the resonant Raman spectrum of MB solution (blue). These spectral changes might be induced by MB-AuNP binding and subsequent silica shell enclosure, which did not affect the chemical structure of MB. In fact, the SERRS activity of antigen-Ab-SARS-CoV-2-SERRS nanoprobes (green) also demonstrated that MB molecules did not undergo any chemical modification during building of the immunoassay platform and/or with the tests in SERRS detection. The contact between the metallic surface and MB molecules leads to fluorescence quenching, favoring the enhanced Raman signal [62]. Additionally, the spectrum (green) for Ab-SARS-CoV-2-SERRS nanoprobes was not affected in the immunoassay to detect 1 μg/mL of SARS-CoV-2 antigen (antigen-Ab-SARS-CoV-2-SERRS nanoprobes). The SERRS spectra from the SERRS nanoprobes and antigen-Ab-SARS-CoV-2-SERRS nanoprobes display slight changes in intensity and band position, with spectral profiles comparable to the resonant Raman spectrum of MB solution (blue; Fig. 2).

The relative intensity of the bands from vibrational modes of N–CH$_3$ symmetrical stretching and C–C ring stretching is inverted when the resonant Raman spectrum of MB solution is compared with the SERRS spectra of the SERRS nanoprobes and of the antigen-Ab-SARS-CoV-2-

SERRS nanoprobes. In MB solution the band at 1623 cm^{-1} assigned to C–C ring stretching is the most intense with the band at 1396 cm^{-1} assigned to the vibrational mode N–CH$_3$ symmetrical stretching being the second most intense. In the SERRS spectra of SERRS nanoprobes and antigen-Ab-SARS-CoV-2-SERRS nanoprobes, the band from N–CH$_3$ symmetrical stretching (at 1383 cm^{-1}) is the most intense, followed by the band from C–C ring stretching [54]. This might suggest a preferential orientation of MB molecules on the nanoprobes. The enhanced Raman signal is highly dependent on the distance between the adsorbed molecule and metallic surface, and on molecular orientation [63–66]. Therefore, it can be assumed that MB molecules are adsorbed on the AuNP surface through the N–CH$_3$ bond, in a more inclined orientation to the vertical line. The dipole of C–C stretching ring is parallel to $\overrightarrow{E}_{local}$ surrounding the metallic nanoparticle, being perpendicular to its surface. This molecular orientation of MB leads to a maximum enhancement of the 1383 cm^{-1} band (N–CH$_3$ symmetrical stretching) followed by the band at 1623 cm^{-1} (C–C ring stretching), respectively. A proposal for the orientation of MB molecules on the AuNP is given in Figure S1 (Supplementary Material).

Different concentrations of SARS-CoV-2 antigen (from 100 μg/mL to 0.01 ng/mL) were studied by incubating the Ab-SARS-CoV-2 functionalized cover slides with the antigens for 1 h and with Ab-SARS-CoV-2-SERRS nanoprobes for another 1 h. The SERRS mappings taken are plotted in Fig. 3(a)-(h). Control experiments were performed without the antigen ("No antigen": SERRS nanoprobes dropped directly onto the cover slide functionalized with SARS-CoV-2 antibodies, incubation for 1 h, followed by rinsing with PBS solution) and in the absence of antigens and SERRS nanoprobes ("Blank": only the cover slide functionalized with SARS-CoV-2 antibodies). The SERRS mapping is made by delimiting an area on the immunoassay platform and collecting SERRS spectra point-by-point along the defined area. For Fig. 3 we delimited a square of 40×40 μm^2 with a 3 μm step, generating a total of 196 SERRS spectra per mapping. Each SERRS mapping was plotted by taking the band intensity at 1383 cm^{-1} (peak intensity without any baseline correction) (Fig. 3), where the brighter spots refer to higher intensities. This band was chosen owing to its high intensity; it is assigned to the vibrational mode of N–CH$_3$ symmetrical stretching, which is covalently bonded to Au surface (Fig. 3(k)). The distribution of SERRS intensities indicates that the nanoprobes are fairly dispersed on the platform surface. SARS-CoV-2 antigen was detected at every probed concentration (Fig. 3(a)–(h)). The lowest concentration of SARS-CoV-2 antigen was 0.01 ng/mL (0.13 pM), smaller than the concentrations reported with recent methodologies to detect COVID-19. Indeed, the detection limits were 5 ng/mL for lateral flow via ACE2 receptor [72], 12.6 nM for single-walled carbon nanotube (SWCNT)-based fluorescence sensing [73], 50 pg/mL for microfluidic magneto immunosensor using electrochemical measurements [13], and 0.22 pM for plasmonic photothermal biosensors [74].

The SERRS intensity at 1383 cm^{-1} was averaged from a total of 196 SERRS spectra recorded in triplicate for each concentration of SARS-CoV-2 antigen, from which the adsorption curve in Fig. 4(a) was obtained. The isotherm could be fitted with the Langmuir adsorption model [75–77] for the range of detection analyzed here, from 100 μg/mL to 0.01 ng/mL of SARS-CoV-2 spike glycoprotein (S1) (coefficient of determination, $R^2 = 0.9604$). At low concentrations (from 100 ng/mL to 0.01 ng/mL) the increase in SERRS intensity with the SARS-CoV-2 antigen concentration could be approximated with a linear function, as shown in Fig. 4(b) (coefficient of determination, $R^2 = 0.9741$). At this linear regime, no intermolecular interactions are predicted to occur and a calibration curve was used to determine the limit of detection (LOD) of the SERRS immunoassay platform [76,78]. LOD was calculated according to the following equation [48,77,79,80]:

$$LOD = 3 \times SD_{Blank}/b$$

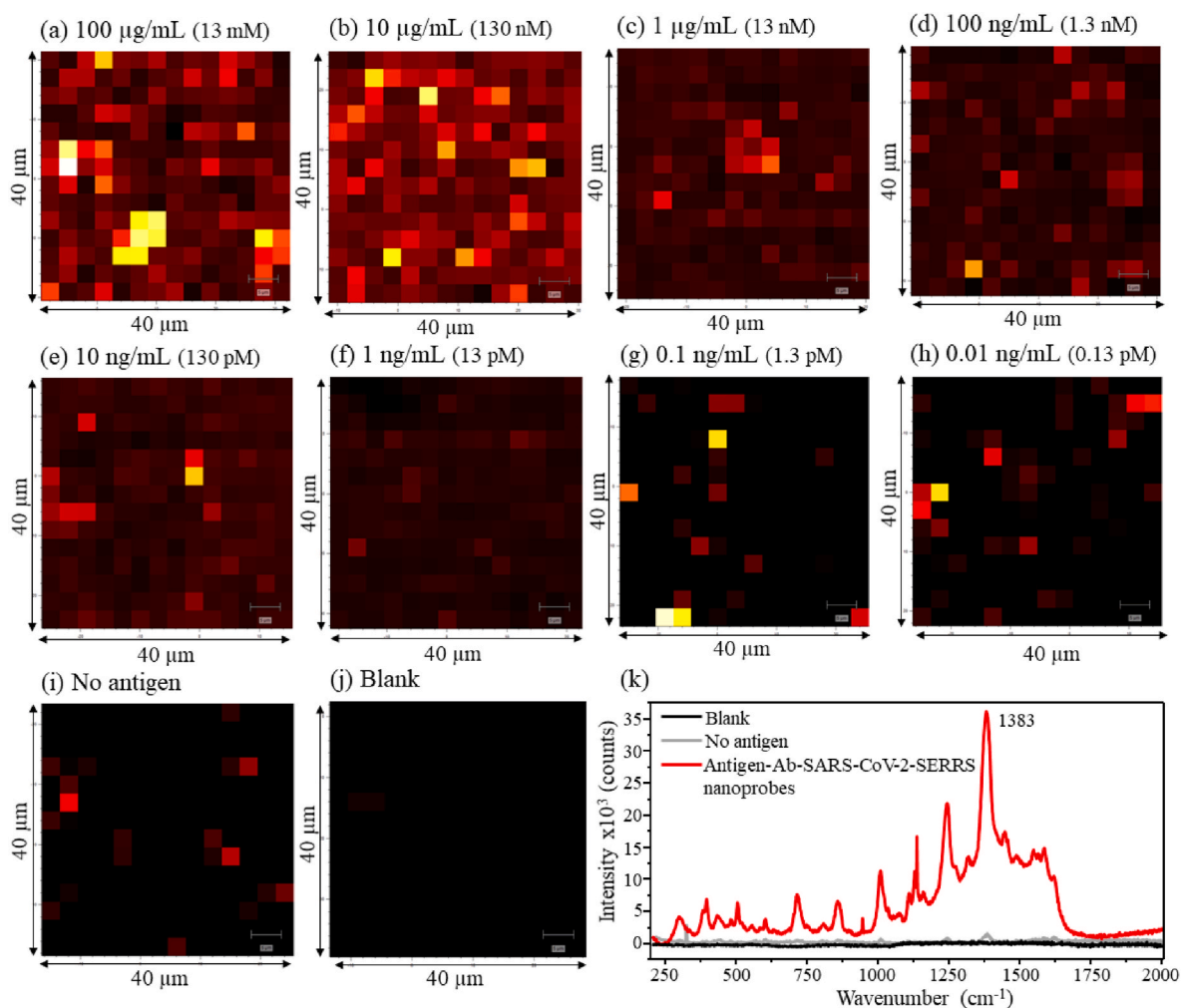where SD_{Blank} is the standard deviation of the "Blank" sample and b is

Fig. 3. SERRS area mappings (40 μm × 40 μm and step of 3 μm) show the intensity distribution (peak intensity without any treatment) of the band at 1383 cm^{-1} for (a)–(h) different concentrations of SARS-CoV-2 antigen, (i) in the absence of antigen ("No antigen") and (j) without antigen and with no SERRS nanoprobes ("Blank"). The same color scale was set for all SERRS mappings. (k) Raman spectra for the control experiments, "Blank" and "No antigen", and SERRS spectrum (with baseline correction) for the antigen-Ab-SARS-CoV-2-SERRS nanoprobes detecting 100 μg/mL of antigen. Excitation laser at 633 nm. (For interpretation of the references to color in this figure legend, the reader is referred to the Web version of this article.)
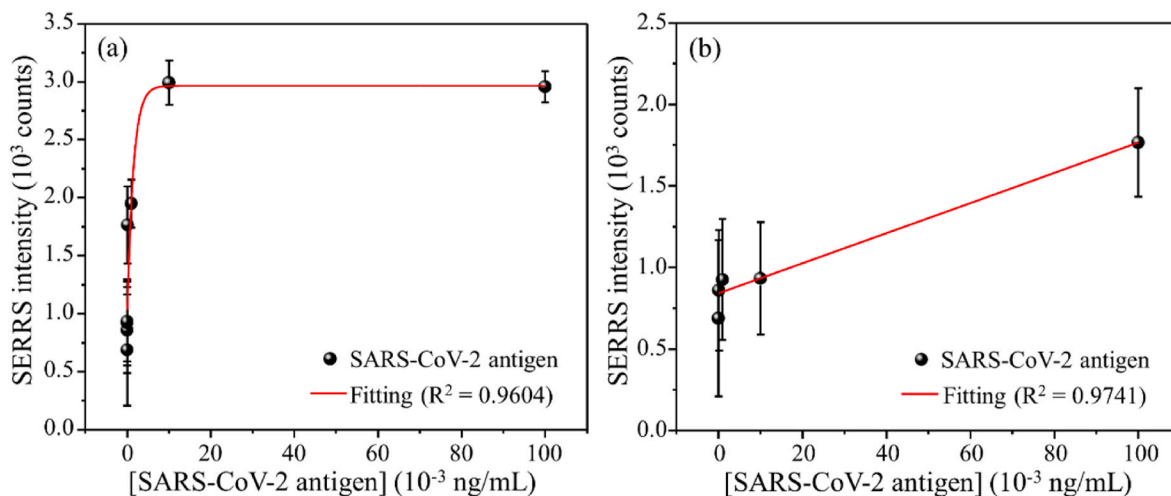

Fig. 4. (a) Langmuir adsorption isotherm between the SERRS intensity (at 1383 cm^{-1}) and concentration of SARS-CoV-2 antigen, from 100 μg/mL to 0.01 ng/mL. The SERRS intensity is an average of the 196 SERRS spectra recorded in triplicate for each concentration of SARS-CoV-2 antigen, and the error bars represent the standard deviation. (b) Details at lower concentrations (from 100 ng/mL to 0.01 ng/mL), where the SERRS intensity increases linearly with the SARS-CoV-2 antigen concentration.

Table 2
Summary of the LOD for SARS-CoV-2 spike (S1) protein found in published research in comparison with our SERRS immunoassay platform.

Type of sensor	Limit of detection (LOD)	Reference
Electrochemical immunosensor	20 ng/mL	[49]
Paper-based sensor	[0.030 nM]	[81]
Gold-nanoarchitecture-assisted laser-scribed graphene biosensor	2.9 ng/mL	[82]
SERRS immunoassay platform	0.046 ng/mL [0.60 pM]	[Current approach]

the slope of the calibration curve. The LOD (0.046 ng/mL or 0.60 pM) obtained here is compared in Table 2 with published research results of detection of SARS-CoV-2 spike glycoprotein (S1). For instance, our SERRS immunoassay platform was capable to detect the antigen at lower concentrations than with enzyme-linked immunoassay (ELISA) for spike (S1) protein in recombinant SARS-CoV-2 using electrochemical techniques, which was 20 ng/mL [49]. The detection of SARS-CoV-2 antigen at picomolar concentration is possible due to the enhancement in MB resonance Raman signal enabled by SERRS nanoprobes. This sensitivity permits detection of viral proteins at the onset of symptoms, as expected from the ca. 8 pg/mL concentration of SARS-CoV-2 spike (S1) protein in the plasma of COVID-19 patients [28]. Therefore, the sensitivity, photostability and rapid accuracy of the SERRS immunoassay designed here confirm the potential for detecting low SARS-CoV-2 antigen concentrations, relevant for early diagnosis.

In order to make the analysis of SERRS mapping more quantitative, we employed the multidimensional projection technique referred to as Sammon's mapping [51,52]. In this technique, the data from a high-dimensional space are mapped onto a lower dimension space where the similarity relationships among data instances in the high-dimensional space should be preserved [52]. Each circle in Fig. 5 represents an average of the whole 196 spectra of the SERRS area mapping displayed in Fig. 3, for each antigen concentration. The Sammon's mapping was performed without any previous treatment on the SERRS spectra. The proximity of the circles is an indication of similarity among the SERRS mapping response. The different concentrations of SARS-CoV-2 antigen are positioned in three principal groups (µg/mL, ng/mL, and lowest concentrations (ng/mL)), with exception of the concentration at 1 µg/mL. Even within these groups, the concentrations are relatively apart from each other, confirming the ability of the multidimensional projection in distinguishing the SERRS mappings of different concentrations. Besides, the separation from the controls "no antigen" and "blank" group is increased with increasing antigen concentration from 0.01 ng/mL to 100 µg/mL, confirming the distinguishing ability of the immunoassay platform. In particular, the "no antigen" and "blank" group are closer to the group of lowest concentrations (0.1 and 0.01 ng/mL), comparable to that in Fig. 3.

We also performed interferents analysis using the pharmaceutical drugs: paracetamol, azithromycin, dexamethasone and ivermectin,

which have been used against COVID-19, though considered ineffective. The Sammon's mapping data plotted in Fig. 5 includes the different concentrations of SARS-CoV-2 antigen and the 4 interferents (separately and mixed). The different concentrations of SARS-CoV-2 antigen are easily distinguishable from each other and positioned apart from the data of the interferents. They are grouped on the bottom right of the Sammon's mapping, highlighting the ability of our SERRS immunoassay platform to also distinguish interferents. Soares et al. [22] developed a biosensor capable to differentiate various concentrations of SARS-CoV-2 antigen from control experiments (interferents) applying IDMAP technique to analyze electrical impedance spectroscopy measurements. Moreover, SARS-CoV-2 antigens embedded into to the interferents could also be discriminated, as shown in Figure S2.

4. Conclusions

The surface-enhanced resonance Raman scattering (SERRS) immunoassay platform designed here was able to detect trace levels of viral spike (S1) glycoprotein from SARS-CoV-2, with a limit of detection (LOD) of 0.046 ng/mL (0.60 pM). This was made possibly by exploiting SERRS on the Raman reporter methylene blue (MB) wrapped between AuNPs and a silica layer (SERRS nanoprobe). Specificity to the spike protein of SARS-CoV-2 was warranted by functionalizing the nanoprobe with SARS-CoV-2 antibodies, in addition to the functionalization of the cover slide with the same antibodies. The selectivity of the immunosensor was confirmed by treating the SERRS spectra of control solutions, various concentrations of the spike protein and interferents with the Sammon's mapping multidimensional projection technique. It is significant that detection can be made of spike protein concentrations comparable to the lowest concentration found in the plasma of COVID-19 patients (8 pg/mL) at the onset of symptoms. With these proof-of-concept experiments, we demonstrated the viability of early diagnosis of COVID-19 using SERRS. No attempt was made to optimize the fabrication of the immunoassay platform, e.g. with regard to the time taken for the test. As it is now, the test takes at least 2 h and requires a rather sophisticated instrument (Raman spectrometer). However, this time may be shortened with optimization procedures which could also enhance sensitivity. Furthermore, it is possible to employ portable Raman spectrometers, and this would decrease the cost of the tests considerably.

Credit author statement

Maria J. Bistaffa: Formal analysis, Investigation, Validation, Visualization, Writing – original draft, Writing - review & editing. **Sabrina A. Camacho**: Conceptualization, Formal analysis, Investigation, Methodology, Validation, Visualization, Writing – original draft, Writing - review & editing. **Wallance M. Pazin**: Formal analysis, Investigation, Methodology, Validation, Visualization, Writing - review & editing. **Carlos J. L. Constantino**: Writing - review & editing, Resources,
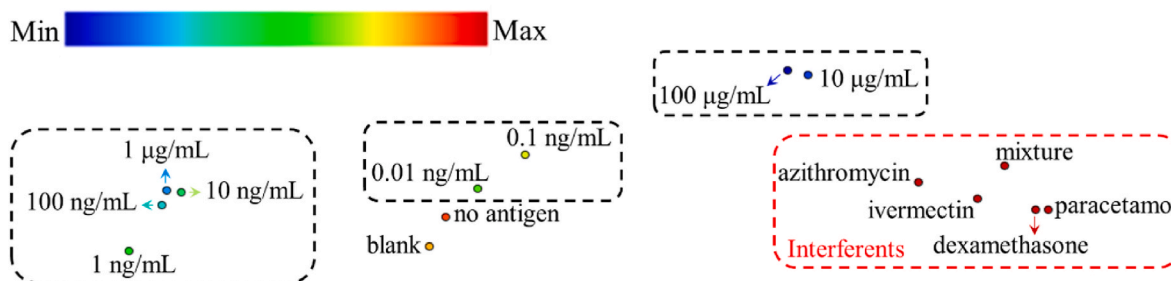
Fig. 5. Sammon's mapping for different concentrations of SARS-CoV-2 antigen and for the interferents paracetamol, azithromycin, dexamethasone, ivermectin and mixed interferents. The controls "No antigen" and "Blank" were also evaluated. Each circle represents the average of the 196 SERRS spectra for each mapping of a given antigen concentration, without any spectral treatment. The proximity of the circles indicates the similarity between the data (i.e., similar the SERRS mappings responses will lead to circles closer to each other).

Supervision, Project administration, Funding acquisition. **Osvaldo N. Oliveira Jr.**: Writing - review & editing, Resources, Supervision, Project administration, Funding acquisition. **Pedro H. B. Aoki**: Conceptualization, Methodology, Formal analysis, Writing - Review & Editing, Resources, Supervision, Project administration, Funding acquisition.

Declaration of competing interest

The authors declare that they have no known competing financial interests or personal relationships that could have appeared to influence the work reported in this paper.

Acknowledgments

Appendix A. Supplementary data

Supplementary data to this article can be found online at https://doi.org/10.1016/j.talanta.2022.123381.

References

[1] Worldometers, Coronavirus Update (Live) Cases and Deaths from Covid-19 Virus Pandemic, 2021.

[2] Johns Hopkins Coronavirus Resource, Covid-19 Map, 2021.

[3] World Health Organization, Rolling Updates on Coronavirus Disease (Covid-19), 2021.

[4] C.-C. Lai, T.-P. Shih, W.-C. Ko, H.-J. Tang, P.-R. Hsueh, Severe acute respiratory syndrome coronavirus 2 (SARS-CoV-2) and coronavirus disease-2019 (Covid-19): the epidemic and the challenges, Int. J. Antimicrob. Agents 55 (2020) 105924, https://doi.org/10.1016/j.ijantimicag.2020.105924.

[5] L. Xie, F. Liu, J. Liu, H. Zeng, A nanomechanical study on deciphering the stickiness of SARS-CoV-2 on inanimate surfaces, ACS Appl. Mater. Interfaces 12 (2020) 58360–58368, https://doi.org/10.1021/acsami.0c16800.

[6] S.M. Kissler, C. Tedijanto, E. Goldstein, Y.H. Grad, M. Lipsitch, Projecting the transmission dynamics of SARS-CoV-2 through the postpandemic period, Science 368 (2020) 860–868, https://doi.org/10.1126/science.abb5793.

[7] I.A. Mattioli, A. Hassan, O.N. Oliveira Jr., F.N. Crespilho, On the challenges for the diagnosis of SARS-CoV-2 based on a review of current methodologies, ACS Sens. 5 (2020) 3655–3677, https://doi.org/10.1021/acssensors.0c01382.

[8] S.A. Bustin, T. Nolan, RT-qPCR testing of SARS-CoV-2: a primer, Int. J. Mol. Sci. 21 (2020) 3004, https://doi.org/10.3390/ijms21083004.

[9] C.P. West, V.M. Montori, P. Sampathkumar, Covid-19 testing: the threat of false-negative results, Mayo Clin. Proc. 95 (2020) 1127–1129, https://doi.org/10.1016/j.mayocp.2020.04.004.

[10] R. Wölfel, V.M. Corman, W. Guggemos, M. Seilmaier, S. Zange, M.A. Müller, D. Niemeyer, T.C. Jones, P. Vollmar, C. Rothe, M. Hoelscher, T. Bleicker, S. Brünink, J. Schneider, R. Ehmann, K. Zwirglmaier, C. Drosten, C. Wendtner, Virological assessment of hospitalized patients with Covid-19, Nature 581 (2020) 465–469, https://doi.org/10.1038/s41586-020-2196-x.

[11] Y. Fang, H. Zhang, J. Xie, M. Lin, L. Ying, P. Pang, W. Ji, Sensitivity of chest CT for Covid-19: comparison to RT-PCR, Radiology 296 (2020), https://doi.org/10.1148/radiol.2020200432. E115–E117.

[12] W. Zhang, R.-H. Du, B. Li, X.-S. Zheng, X.-L. Yang, B. Hu, Y.-Y. Wang, G.-F. Xiao, B. Yan, Z.-L. Shi, P. Zhou, Molecular and serological investigation of 2019-nCoV infected patients: implication of multiple shedding routes, Emerg, Microb. Infect. 9 (2020) 386–389, https://doi.org/10.1080/22221751.2020.1729071.

[13] J. Li, P.B. Lillehoj, Microfluidic magneto immunosensor for rapid, high sensitivity measurements of SARS-CoV-2 nucleocapsid protein in serum, ACS Sens. 6 (2021) 1270–1278, https://doi.org/10.1021/acssensors.0c02561.

[14] J.T. Heggestad, D.S. Kinnamon, L.B. Olson, J. Liu, K. Garrett, S.A. Wall, C. M. Fontes, D.Y. Joh, A.M. Hucknall, C. Pieper, I.A. Naqvi, L. Chen, L.G. Que, T. Oguin, S.K. Nair, B.A. Sullenger, C.W. Woods, G.D. Sempowski, B.D. Kraft, A. Chilkoti, Multiplexed, quantitative serological profiling of Covid-19 from blood by a point-of-care test, Sci. Adv. 7 (2021), eabg4901, https://doi.org/10.1126/sciadv.abg4901.

[15] P. Zhang, Q. Gao, T. Wang, Y. Ke, F. Mo, R. Jia, W. Liu, L. Liu, S. Zheng, Y. Liu, L. Li, Y. Wang, L. Xu, K. Hao, W. Min, X. Liu, R. Yang, S. Li, C. Lin, Y. Zhao, Development and evaluation of a serological test for diagnosis of Covid-19 with selected recombinant spike proteins, Eur. J. Clin. Microbiol. Infect. Dis. 40 (2021) 921–928, https://doi.org/10.1007/s10096-020-04102-4.

[16] F. Bonelli, A. Sarasini, C. Zierold, M. Calleri, A. Bonetti, C. Vismara, F.A. Blocki, L. Pallavicini, A. Chinali, D. Campisi, E. Percivalle, A.P. DiNapoli, C.F. Perno, F. Baldanti, Clinical and analytical performance of an automated serological test that identifies S1/S2-neutralizing IgG in covid-19 patients semiquantitatively, J. Clin. Microbiol. 58 (2020), https://doi.org/10.1128/JCM.01224-20 e01224-20.

[17] S.-Y. Xiao, Y. Wu, H. Liu, Evolving status of the 2019 novel coronavirus infection: proposal of conventional serologic assays for disease diagnosis and infection monitoring, J. Med. Virol. 92 (2020) 464–467, https://doi.org/10.1002/jmv.25702.

[18] L. Guo, L. Ren, S. Yang, M. Xiao, D. Chang, F. Yang, C.S. Dela Cruz, Y. Wang, C. Wu, Y. Xiao, L. Zhang, L. Han, S. Dang, Y. Xu, Q.-W. Yang, S.-Y. Xu, H.-D. Zhu, Y.-C. Xu, Q. Jin, L. Sharma, L. Wang, J. Wang, Profiling early humoral response to diagnose novel coronavirus disease (Covid-19), Clin. Infect. Dis. 71 (2020) 778–785, https://doi.org/10.1093/cid/ciaa310.

[19] W. Liu, L. Liu, G. Kou, Y. Zheng, Y. Ding, W. Ni, Q. Wang, L. Tan, W. Wu, S. Tang, Z. Xiong, S. Zheng, Evaluation of nucleocapsid and spike protein-based enzyme-linked immunosorbent assays for detecting antibodies against SARS-CoV-2, J. Clin. Microbiol. 58 (2020), https://doi.org/10.1128/JCM.00461-20, 00461–20.

[20] J. Zhao, Q. Yuan, H. Wang, W. Liu, X. Liao, Y. Su, X. Wang, J. Yuan, T. Li, J. Li, S. Qian, C. Hong, F. Wang, Y. Liu, Z. Wang, Q. He, Z. Li, B. He, T. Zhang, Y. Fu, S. Ge, L. Liu, J. Zhang, N. Xia, Z. Zhang, Antibody responses to SARS-CoV-2 in patients with novel coronavirus disease 2019, Clin. Infect. Dis. 71 (2020) 2027–2034, https://doi.org/10.1093/cid/ciaa344.

[21] Z. Li, Y. Yi, X. Luo, N. Xiong, Y. Liu, S. Li, R. Sun, Y. Wang, B. Hu, W. Chen, Y. Zhang, J. Wang, B. Huang, Y. Lin, J. Yang, W. Cai, X. Wang, J. Cheng, Z. Chen, K. Sun, W. Pan, Z. Zhan, L. Chen, F. Ye, Development and clinical application of a rapid IgM-IgG combined antibody test for SARS-CoV-2 infection diagnosis, J. Med. Virol. 92 (2020) 1518–1524, https://doi.org/10.1002/jmv.25727.

[22] J.C. Soares, A.C. Soares, M.K.S.C. Angelim, J.L. Proença-Modena, P.M. Moraes-Vieira, L.H.C. Mattoso, O.N. Oliveira Jr., Diagnostics of SARS-CoV-2 infection using electrical impedance spectroscopy with an immunosensor to detect the spike protein, Talanta 239 (2022) 123076, https://doi.org/10.1016/j.talanta.2021.123076.

[23] S.H. Lee, Y.K. Lee, S.-H. Lee, J. Kwak, H.S. Song, M. Seo, Detection and discrimination of SARS-CoV-2 spike protein-derived peptides using THz metamaterials, Biosens. Bioelectron. 202 (2022) 113981, https://doi.org/10.1016/j.bios.2022.113981.

[24] C.C. Mayorga-Martinez, J. Vyskočil, F. Novotný, P. Bednar, D. Ruzek, O. Alduhaish, M. Pumera, Collective behavior of magnetic microrobots through immuno-sandwich assay: on-the-fly Covid-19 sensing, Appl. Mater. Today. 26 (2022) 101337, https://doi.org/10.1016/j.apmt.2021.101337.

[25] P.-H. Chen, C.-C. Huang, C.-C. Wu, P.-H. Chen, A. Tripathi, Y.-L. Wang, Saliva-based Covid-19 detection: a rapid antigen test of SARS-CoV-2 nucleocapsid protein using an electrical-double-layer gated field-effect transistor-based biosensing system, Sensor. Actuator. B Chem. 357 (2022) 131415, https://doi.org/10.1016/j.snb.2022.131415.

[26] H. Qi, Z. Hu, Z. Yang, J. Zhang, J.J. Wu, C. Cheng, C. Wang, L. Zheng, Capacitive aptasensor coupled with microfluidic enrichment for real-time detection of trace SARS-CoV-2 nucleocapsid protein, Anal. Chem. 94 (2022) 2812–2819, https://doi.org/10.1021/acs.analchem.1c04296.

[27] X. Lu, H. Lee Yu, H. Lin, Y. Cao, I.-M. Hsing, Rapid and highly specific detection of communicable pathogens using one-pot loop probe-mediated isothermal amplification (oLAMP), Sensor. Actuator. B Chem. 357 (2022) 131385, https://doi.org/10.1016/j.snb.2022.131385.

[28] A.F. Ogata, A.M. Maley, C. Wu, T. Gilboa, M. Norman, R. Lazarovits, C.-P. Mao, G. Newton, M. Chang, K. Nguyen, M. Kamkaew, Q. Zhu, T.E. Gibson, E.T. Ryan, R. C. Charles, W.A. Marasco, D.R. Walt, Ultra-sensitive serial profiling of SARS-CoV-2 antigens and antibodies in plasma to understand disease progression in Covid-19 patients with severe disease, Clin. Chem. 66 (2020) 1562–1572, https://doi.org/10.1093/clinchem/hvaa213.

[29] T. Nagy-Simon, A.-M. Hada, S. Suarasan, M. Potara, Recent advances on the development of plasmon-assisted biosensors for detection of C-reactive protein, J. Mol. Struct. 1246 (2021) 131178, https://doi.org/10.1016/j.molstruc.2021.131178.

[30] J.R. Mejía-Salazar, S.A. Camacho, C.J.L. Constantino, O.N. Oliveira Jr., New trends in plasmonic (Bio)sensing, An. Acad. Bras. Cienc. 90 (2018) 779–801, https://doi.org/10.1590/0001-3765201820170571.

[31] A. Hariharan, P. Vadlamudi, SERS of Epinephrine: a computational and experimental study, J. Mol. Struct. 1246 (2021) 131163, https://doi.org/10.1016/j.molstruc.2021.131163.

[32] J. Ko, J. Ham, H. Lee, K. Lee, W.-G. Koh, Integration of a fiber-based cell culture and biosensing system for monitoring of multiple protein markers secreted from stem cells, Biosens. Bioelectron. 193 (2021) 113531, https://doi.org/10.1016/j.bios.2021.113531.

[33] Y. Lin, S. Gao, M. Zheng, S. Tang, K. Lin, S. Xie, Y. Yu, J. Lin, A microsphere nanoparticle based-serum albumin targeted adsorption coupled with surface-enhanced Raman scattering for breast cancer detection, Spectrochim. Acta Part A Mol. Biomol. Spectrosc. 261 (2021), https://doi.org/10.1016/j.saa.2021.120039, 120039.

[34] J. Lei, D. Yang, R. Li, Z. Dai, C. Zhang, Z. Yu, S. Wu, L. Pang, S. Liang, Y. Zhang, Label-free surface-enhanced Raman spectroscopy for diagnosis and analysis of serum samples with different types lung cancer, Spectrochim. Acta Part A Mol. Biomol. Spectrosc. 261 (2021) 120021, https://doi.org/10.1016/j.saa.2021.120021.

[35] X. Tian, Q. Fan, J. Guo, Q. Yu, L. Xu, X. Kong, Surface-enhanced Raman scattering of flexible cotton fiber-Ag for rapid adsorption and detection of malachite green in fish, Spectrochim. Acta Part A Mol. Biomol. Spectrosc. 263 (2021), https://doi.org/10.1016/j.saa.2021.120174, 120174.

[36] J. Tang, Q. Zhang, J. Zhou, H. Fang, H. Yang, F. Wang, Investigation of pesticide residue removal effect of gelatinized starch using surface-enhanced Raman scattering mapping, Food Chem 365 (2021) 130448, https://doi.org/10.1016/j.foodchem.2021.130448.

[37] K. Wang, J. Li, Reliable SERS detection of pesticides with a large-scale self-assembled Au@4-MBA@Ag nanoparticle array, Spectrochim. Acta Part A Mol. Biomol. Spectrosc. 263 (2021) 120218, https://doi.org/10.1016/j.saa.2021.120218.

[38] S. Kamal, T.C.-K. Yang, Silver enriched silver phosphate microcubes as an efficient recyclable SERS substrate for the detection of heavy metal ions, J. Colloid Interface Sci. 605 (2022) 173–181, https://doi.org/10.1016/j.jcis.2021.07.084.

[39] Y. Lin, J. Gao, S. Tang, X. Zhao, M. Zheng, W. Gong, S. Xie, S. Gao, Y. Yu, J. Lin, Label-free diagnosis of breast cancer based on serum protein purification assisted surface-enhanced Raman spectroscopy, Spectrochim. Acta Part A Mol. Biomol. Spectrosc. 263 (2021) 120234, https://doi.org/10.1016/j.saa.2021.120234.

[40] M. Zhang, X. Li, J. Pan, Y. Zhang, L. Zhang, C. Wang, X. Yan, X. Liu, G. Lu, Ultrasensitive detection of SARS-CoV-2 spike protein in untreated saliva using SERS-based biosensor, Biosens. Bioelectron. 190 (2021) 113421, https://doi.org/10.1016/j.bios.2021.113421.

[41] Q. Qu, J. Wang, C. Zeng, M. Wang, W. Qi, Z. He, AuNP array coated substrate for sensitive and homogeneous SERS-immunoassay detection of human immunoglobulin G, RSC Adv 11 (2021) 22744–22750, https://doi.org/10.1039/d1ra02404c.

[42] J. Turkevich, P.C. Stevenson, J. Hillier, A study of the nucleation and growth processes in the synthesis of colloidal gold, Discuss. Faraday Soc. 11 (1951) 55, https://doi.org/10.1039/df9511100055.

[43] M. Li, J.W. Kang, S. Sukumar, R.R. Dasari, I. Barman, Multiplexed detection of serological cancer markers with plasmon-enhanced Raman spectro-immunoassay, Chem. Sci. 6 (2015) 3906–3914, https://doi.org/10.1039/c5sc01054c.

[44] B. Tang, J. Wang, J.A. Hutchison, L. Ma, N. Zhang, H. Guo, Z. Hu, M. Li, Y. Zhao, Ultrasensitive, multiplex Raman frequency shift immunoassay of liver cancer biomarkers in physiological media, ACS Nano 10 (2016) 871–879, https://doi.org/10.1021/acsnano.5b06007.

[45] R.F. Aroca, G.Y. Teo, H. Mohan, A.R. Guerrero, P. Albella, F. Moreno, Plasmon-enhanced fluorescence and spectral modification in SHINEF, J. Phys. Chem. C 115 (2011) 20419–20424, https://doi.org/10.1021/jp205997u.

[46] J.F. Li, X.D. Tian, S.B. Li, J.R. Anema, Z.L. Yang, Y. Ding, Y.F. Wu, Y.M. Zeng, Q. Z. Chen, B. Ren, Z.L. Wang, Z.Q. Tian, Surface analysis using shell-isolated nanoparticle-enhanced Raman spectroscopy, Nat. Protoc. 8 (2013) 52–65, https://doi.org/10.1038/nprot.2012.141.

[47] S.A. Camacho, R.G. Sobral-Filho, P.H.B. Aoki, C.J.L. Constantino, A.G. Brolo, Immunoassay quantification using surface-enhanced fluorescence (SEF) tags, Analyst 142 (2017) 2717–2724, https://doi.org/10.1039/c7an00639j.

[48] S.A. Camacho, R.G. Sobral-Filho, P.H.B. Aoki, C.J.L. Constantino, A.G. Brolo, Zika immunoassay based on surface-enhanced Raman scattering nanoprobes, ACS Sens. 3 (2018) 587–594, https://doi.org/10.1021/acssensors.7b00639.

[49] B. Mojsoska, S. Larsen, D.A. Olsen, J.S. Madsen, I. Brandslund, F.A. Alatraktchi, Rapid SARS-CoV-2 detection using electrochemical immunosensor, Sensors 21 (2021) 1–11, https://doi.org/10.3390/s21020390.

[50] A. Ahmadivand, B. Gerislioglu, Z. Ramezani, A. Kaushik, P. Manickam, S. A. Ghoreishi, Functionalized terahertz plasmonic metasensors: femtomolar-level detection of SARS-CoV-2 spike proteins, Biosens. Bioelectron. 177 (2021) 112971, https://doi.org/10.1016/j.bios.2021.112971.

[51] R. Minghim, F.V. Paulovich, A. de Andrade Lopes, Content-based text mapping using multi-dimensional projections for exploration of document collections, https://doi.org/10.1117/12.660598 60600S–60600S–12, Proc. SPIE 6060 (2006) 1–12.

[52] J.W. Sammon, A nonlinear mapping for data structure analysis, IEEE Trans. Comput. 18 (1969) 401–409, https://doi.org/10.1109/t-c.1969.222678.

[53] D. Heger, J. Jirkovský, P. Klán, Aggregation of methylene blue in frozen aqueous solutions studied by absorption spectroscopy, J. Phys. Chem. 109 (2005) 6702–6709, https://doi.org/10.1021/jp050439j.

[54] K.-D. Shim, E.-S. Jang, SERS signal enhancement of methylene blue-embedded agglomerated gold nanorod@SiO2 core@shell composites, Bull. Kor. Chem. Soc. 39 (2018) 936–940, https://doi.org/10.1002/bkcs.11528.

[55] S.A. Camacho, M.B. Kobal, A.M. Almeida, K.A. Toledo, O.N. Oliveira Jr., P.H. B. Aoki, Molecular-level effects on cell membrane models to explain the phototoxicity of gold shell-isolated nanoparticles to cancer cells, Colloids Surf. B Biointerfaces 194 (2020) 111189, https://doi.org/10.1016/j.colsurfb.2020.111189.

[56] S.A. Camacho, M.B. Kobal, L.G. Moreira, M.J. Bistaffa, T.C. Roque, W.M. Pazin, K. A. Toledo, O.N. Oliveira Jr., P.H.B. Aoki, The efficiency of photothermal action of gold shell-isolated nanoparticles against tumor cells depends on membrane interactions, Colloids Surf. B Biointerfaces 211 (2022) 112301, https://doi.org/10.1016/j.colsurfb.2021.112301.

[57] A.G. Amit, R.A. Mariuzza, S.E. Phillips, R.J. Poljak, Three-dimensional structure of an antigen-antibody complex, Proc. Natl. Acad. Sci. Unit. States Am. 84 (1987) 8075–8079, https://doi.org/10.1126/science.2426778.

[58] F. Shan, X.Y. Zhang, X.C. Fu, L.J. Zhang, D. Su, S.J. Wang, J.Y. Wu, T. Zhang, Investigation of simultaneously existed Raman scattering enhancement and inhibiting fluorescence using surface modified gold nanostars as SERS probes, Sci. Rep. 7 (2017) 1–10, https://doi.org/10.1038/s41598-017-07311-8.

[59] J. Gersten, A. Nitzan, Spectroscopic properties of molecules interacting with small dielectric particles, J. Chem. Phys. 75 (1981) 1139–1152, https://doi.org/10.1063/1.442161.

[60] S.A. Camacho, P.H.B. Aoki, P. Albella, O.N. Oliveira Jr., C.J.L. Constantino, R. F. Aroca, Increasing the enhancement factor in plasmon-enhanced fluorescence with shell-isolated nanoparticles, J. Phys. Chem. C 120 (2016) 20530–20535, https://doi.org/10.1021/acs.jpcc.5b09215.

[61] P.H.B. Aoki, D. Volpati, W. Caetano, C.J.L. Constantino, Study of the interaction between cardiolipin bilayers and methylene blue in polymer-based Layer-by-Layer and Langmuir films applied as membrane mimetic systems, Vib. Spectrosc. 54 (2010) 93–102, https://doi.org/10.1016/j.vibspec.2010.03.013.

[62] J. Gersten, A. Nitzan, Electromagnetic theory of enhanced Raman scattering by molecules adsorbed on rough surfaces, J. Chem. Phys. 73 (1980) 3023–3037, https://doi.org/10.1063/1.440560.

[63] M. Moskovits, Surface-enhanced spectroscopy, Rev. Mod. Phys. 57 (1985) 783–826, https://doi.org/10.1103/RevModPhys.57.783.

[64] E.C. Le Ru, P.G. Etchegoin, Principles of Surface-Enhanced Raman Spectroscopy and Related Plasmonic Effects, Elsevier, Boston, USA, 2009.

[65] R.F. Aroca, N.P.W. Pieczonka, M. Nazri, Vibrational spectroscopy and surface-enhanced vibrational spectroscopy of carbonaceous materials: from nanotubes to graphite, Opt. Pura Apl. (2007) 187–194.

[66] S.A. Camacho, P.H.B. Aoki, F.F. De Assis, A.M. Pires, K.T. De Oliveira, R.F. Aroca, C.J.L. Constantino, Co-deposition of gold nanoparticles and metalloporphyrin using the Langmuir-blodgett (LB) technique for surface-enhanced Raman scattering (SERS), Appl. Spectrosc. 69 (2015) 451–456, https://doi.org/10.1366/14-07625.

[67] G.-N. Xiao, S.-Q. Man, Surface-enhanced Raman scattering of methylene blue adsorbed on cap-shaped silver nanoparticles, Chem. Phys. Lett. 447 (2007) 305–309, https://doi.org/10.1016/j.cplett.2007.09.045.

[68] T. Xu, X. Wang, Y. Huang, K. Lai, Y. Fan, Rapid detection of trace methylene blue and malachite green in four fish tissues by ultra-sensitive surface-enhanced Raman spectroscopy coated with gold nanorods, Food Control 106 (2019) 106720, https://doi.org/10.1016/j.foodcont.2019.106720.

[69] M. Aioub, M.A. El-Sayed, A real-time surface enhanced Raman spectroscopy study of plasmonic photothermal cell death using targeted gold nanoparticles, J. Am. Chem. Soc. 138 (2016) 1258–1264, https://doi.org/10.1021/jacs.5b10997.

[70] J. Gopal, H.N. Abdelhamid, J.-H. Huang, H.-F. Wu, Nondestructive detection of the freshness of fruits and vegetables using gold and silver nanoparticle mediated graphene enhanced Raman spectroscopy, Sensor. Actuator. B Chem. 224 (2016) 413–424, https://doi.org/10.1016/j.snb.2015.08.123.

[71] R.R. Naujok, R. V Duevel, R.M. Corn, Fluorescence and Fourier Transform surface-enhanced Raman scattering measurements of methylene blue adsorbed onto a sulfur-modified gold electrode, Langmuir 9 (1993) 1771–1774, https://doi.org/10.1021/la00031a026.

[72] J.-H. Lee, M. Choi, Y. Jung, S.K. Lee, C.-S. Lee, J. Kim, J. Kim, N.H. Kim, B.-T. Kim, H.G. Kim, A novel rapid detection for SARS-CoV-2 spike 1 antigens using human angiotensin converting enzyme 2 (ACE2), Biosens. Bioelectron. 171 (2021) 112715, https://doi.org/10.1016/j.bios.2020.112715.

[73] R.L. Pinals, F. Ledesma, D. Yang, N. Navarro, S. Jeong, J.E. Pak, L. Kuo, Y.-C. Chuang, Y.-W. Cheng, H.-Y. Sun, M.P. Landry, Rapid SARS-CoV-2 spike protein detection by carbon nanotube-based near-infrared nanosensors, Nano Lett 21 (2021) 2272–2280, https://doi.org/10.1021/acs.nanolett.1c00118.

[74] M. Mujawar, H. Gohel, S. Bhardwaj, S. Srinivasan, N. Hickman, A. Kaushik, Aspects of nano-enabling biosensing systems for intelligent healthcare; towards Covid-19 management, Mater. Today Chem. 17 (2020) 100306, https://doi.org/10.1016/j.mtchem.2020.100306.

[75] S. Brunauer, L.S. Deming, W.E. Deming, E. Teller, On a theory of the van der Waals adsorption of gases, J. Am. Chem. Soc. 62 (1940) 1723–1732, https://doi.org/10.1021/ja01864a025.

[76] L.N. Furini, S. Sanchez-Cortes, I. López-Tocón, J.C. Otero, R.F. Aroca, C.J. L. Constantino, Detection and quantitative analysis of carbendazim herbicide on Ag nanoparticles via surface-enhanced Raman scattering, J. Raman Spectrosc. 46 (2015) 1095–1101, https://doi.org/10.1002/jrs.4737.

[77] M.J.S. Oliveira, R.J.G. Rubira, L.N. Furini, A. Batagin-Neto, C.J.L. Constantino, Detection of thiabendazole fungicide/parasiticide by SERS: quantitative analysis and adsorption mechanism, Appl. Surf. Sci. 517 (2020) 145786, https://doi.org/10.1016/j.apsusc.2020.145786.

[78] M. Moskovits, J.S. Suh, Surface geometry change in 2-naphthoic acid adsorbed on silver, J. Phys. Chem. 92 (1988) 6327–6329, https://doi.org/10.1021/j100333a030.

[79] R.J.G. Rubira, S.A. Camacho, C.J.L. Constantino, S. Sanchez-Cortes, Increasing the sensitivity of surface-enhanced Raman scattering detection for s-triazine pesticides by taking advantage of interactions with soil humic substances, J. Raman Spectrosc. 53 (2022) 40–48, https://doi.org/10.1002/jrs.6262.

[80] U.S.D. of H. and H. Services, F. and D. Administration, C. for D.E. and R. (CDER), C. for B.E. and R. (CBER), Analytical Procedures and Methods Validation: Chemistry, Manufacturing, and Controls, 2000.

[81] D. Hristov, H. Rijal, J. Gomez-Marquez, K. Hamad-Schifferli, Developing a paper-based antigen assay to differentiate between coronaviruses and SARS-CoV-2 spike variants, Anal. Chem. 93 (2021) 7825–7832, https://doi.org/10.1021/acs.analchem.0c05438.

[82] T. Beduk, D. Beduk, J.I. de Oliveira Filho, F. Zihnioglu, C. Cicek, R. Sertoz, B. Arda, T. Goksel, K. Turhan, K.N. Salama, S. Timur, Rapid point-of-care Covid-19 diagnosis with a gold-nanoarchitecture-assisted laser-scribed graphene biosensor, Anal. Chem. 93 (2021) 8585–8594, https://doi.org/10.1021/acs.analchem.1c01444.